Electronic Supplementary Information

Multi-Electron Bipolar-Type Organic Molecules for High-Capacity Dual-Ion Zinc Batteries

Chengmin Hu,[a] Xiaozhe Yang,[a] Pingxuan Liu, [a] Ziyang Song, [a] Yaokang Lv,[b] Ling Miao, *[a] Mingxian Liu,*[a] Lihua Gan*[a]

[a] Shanghai Key Laboratory of Chemical Assessment and Sustainability, School of Chemical Science and Engineering, Tongji University, Shanghai 200092, P. R. China.

[b] Zhejiang College of Chemical Engineering, Zhejiang University of Technology, Hangzhou 310014, P. R. China.

*E-mail: 22169@tongji.edu.cn (L. Miao), ganlh@tongji.edu.cn (L. Gan), liumx@tongji.edu.cn (M. Liu).

Table of Contents

Section S1. Experimental Procedures and Calculation Methods.

1.1 Experimental Section.

1.2 Characterization.

1.3 Electrochemical Tests.

1.4 Density functional theory (DFT) calculation.

Section S2. Supporting Characterization Results.

Fig. S1. FT-IR spectra of IDT and AQ.

Fig. S2. Solid-state UV–vis spectra of IDT and AQ.

Fig. S3. The calculated electrical conductivity of AQ and IDT.

Fig. S4. SEM images of IDT and AQ.

Fig. S5. TGA curves of AQ and IDT.

Fig. S6. GCD curves of AQ cathode.

Fig. S7. GCD curves of IDT and AQ cathodes at 10 A g^{-1}.

Fig. S8. Cycling stability and coulombic efficiency of Zn//AQ battery.

Fig. S9. SEM images of Zn anodes before and after cycles.

Table S1. Comparison of rate capacity, energy density and cycling performance of recently reported organic cathode materials for ZIBs in the literatures.

Fig. S10. Capacitive contribution of AQ cathode at 20 mV s^{-1}.

Fig. S11. CV curves of IDT and AQ.

Fig. S12. *Ex-situ* XPS spectra of IDT cathode at various discharged/charged states.

Fig. S13. CV curves of IDT at $ZnSO_4/H_2O$ electrolyte.

Fig. S14. *Ex-situ* XRD patterns.

Fig. S15. GCD curves of IDT cathode at 0.3 M $Zn(OTF)_2$/acetonitrile electrolyte.

Fig. S16. GCD curves of IDT cathode at HOTF electrolytes with different pH values.

Fig. S17. ESP plots of IDT and AQ.

Section S1. Experimental procedures and calculation methods

1.1 Experimental Section

The Zn batteries (CR2032) are assembled using commercial zinc foil as an anode, glass fiber membrane, and 2 M Zn(OTF)$_2$ aqueous electrolyte. The preparation steps of the positive electrode material AQ and IDT are as follows: AQ and IDT are used as the active substance, PTFE is used as the binder, and super P conductive agents are selected, and the slurry is prepared by mixing them in an ethanol dispersant in a mass ratio of 6 : 3 : 1. Then, the obtained slurry is dried in an 80 °C vacuum oven to remove the solvent. The dried slurry was uniformly loaded on the stainless-steel mesh (the mass loading of active materials in the cathode is ~1.0 mg cm^{-2}). Then, we further increased the mass loading to 4, 8, and 10 mg cm^{-2} for high mass-loading electrochemical performance tests, respectively.

1.2 Characterization

The sample morphology was observed by field-emission scanning electron microscopy (SEM, Hitachi S-4800) and transmission electron microscopy (TEM, JEM-2100). The elemental mapping characterization was carried out on a JEM-F200 instrument equipped with an energy diffraction system. Fourier-transformed infrared spectrum (FT-IR) was collected through a Thermo Nicolet NEXUS spectrometer. X-ray diffraction test was performed to analyze the material structure using X-ray diffraction (XRD, Bruker D8 advance powder diffractometer with a Cu Kα radiation source). X-ray photoelectron spectrometer (XPS, AXIS Ultra DLD) was utilized to study the surface chemistry of the samples. Thermogravimetric (TG) analysis was performed with an STA409 PC thermogravimetric analyzer in a nitrogen atmosphere at a heating speed of 10 °C min^{-1}. Nitrogen adsorption/desorption measurements were performed using a Micromeritics ASAP2020 physisorption analyzer at -196 °C. The specific surface area, pore volume, and pore size distribution were evaluated by using the Brunauer-Emmett-Teller (BET) equation and the nonlocal density functional theory model. The ultraviolet-visible (UV-Vis) spectra were obtained with a JASCO V-750 UV-Vis spectrometer.

The optical energy gaps (E_g, eV) of organic cathodes can be determined by ultraviolet-visible (UV-Vis) spectroscopy, which is expressed as:

$$\alpha \propto (h\nu - E_g)^{1/2} / h\nu$$

$$hv = 1240 / \lambda$$

where α denotes the optical absorption coefficient, *hv* is the photon energy, λ is the wavelength.

Before *ex-situ* characterizations, the electrode surface needs to be fine polishing to remove zinc salts. For *ex-situ* characterizations including XPS, XRD, and SEM, the organic cathodes were collected by disassembling the batteries at specific voltages during (dis)charging. After that, the electrodes were rinsed thoroughly with distilled water for 5 times to guarantee the removal of adhered glass fiber and residual electrolyte. Finally, the electrodes were dried in a vacuum oven at 60 °C for 24 h.

1.3 Electrochemical Tests

The cyclic voltammetry (CV) and electrochemical impedance spectroscopy (EIS) measurements with an amplitude of 0.005 V and a test frequency of $10^{-2} \sim 10^{6}$ H_Z were characterized on a CHI660E electrochemical workstation. The equivalent circuit of Nyquist plots includes the equivalent series resistance (R_s), charge transfer resistance (R_{ct}), Warburg impedance (Z_w) and constant phase angle element (CPE). Galvanostatic charge/discharge (GCD) measurements were conducted on the CT3001A battery test system in the potential range of 0−1.6 V. The specific capacity (C_m, mAh g^{-1}) was determined from GCD profiles using the following form:

$$Cm = \frac{I \times \Delta t}{m} \qquad \text{(Eq. S1)}$$

where I, Δt, m refer to the current density (A g^{-1}), the discharging time (s) and the mass loading (g) of active materials on the cathode, respectively.

The gravimetric energy density (E, Wh kg^{-1}) and power density (P, W kg^{-1}) of ZIHCs were estimated based on the following forms:

$$E = C_m \times \Delta V \qquad \text{(Eq. S2)}$$

$$P = E / 1000 \times \Delta t \qquad \text{(Eq. S3)}$$

where ΔV is the voltage window (V).

1.4 Density functional theory (DFT) calculation

Density functional theory (DFT)[S1, S2] was employed to optimize the stabilized structures of AQ

and IDT with Gaussian 09 software package[S3].The B3LYP functional[S4, 5] with 6-31G(d, p) basis sets[S6-8] were selected in all the calculations. On the basis of the optimized structure of AQ/IDT molecule, the electrostatic potential (ESP) analysis on van der Waals surface was done to deduce the possible Zn^{2+} and OTF^- ions uptake positions using the Multiwfn 3.7 software package[S9] and the cubeman utilization in the Gaussian 09 software package. According to the analysis of ESP, the coordination structures of IDT with Zn^{2+} and OTF^- ions were optimized.

Considering thermal correction based on frequency analysis, the binding free energies (ΔG) of every system was the difference of electronic energy. According to frequency and optimization analysis results, the ΔG of the five probable discharging progresses were then calculated.

Section S2. Supporting characterization results
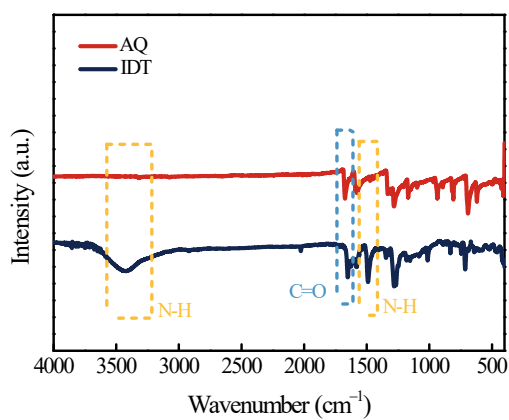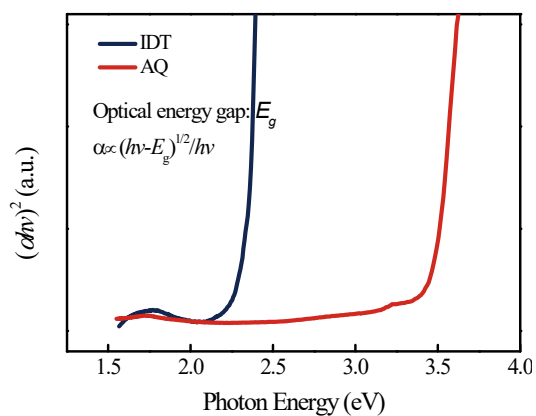
Fig. S1. FT-IR spectra of IDT and AQ.

Fig. S2. Solid-state UV–vis spectra of IDT and AQ.
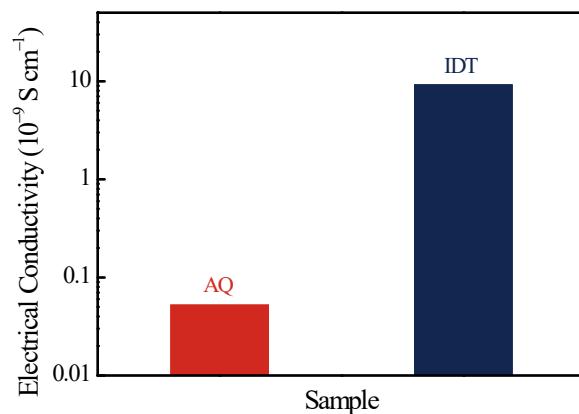
Fig. S3. The calculated electrical conductivity of AQ and IDT.
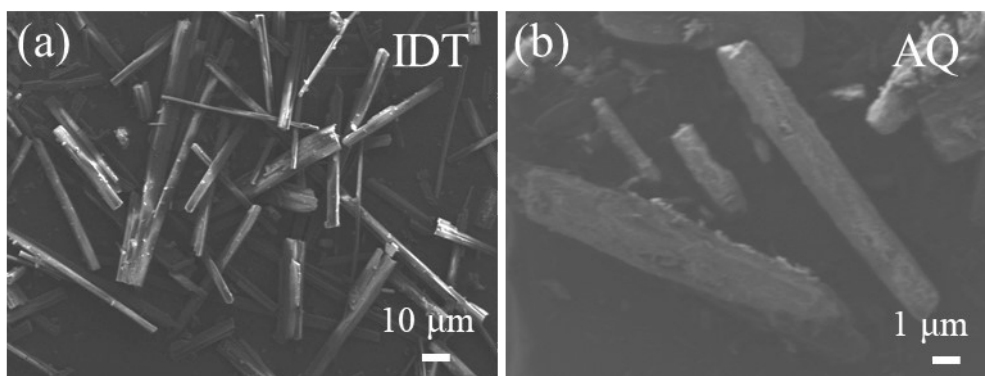
Fig. S4. SEM images of IDT and AQ.
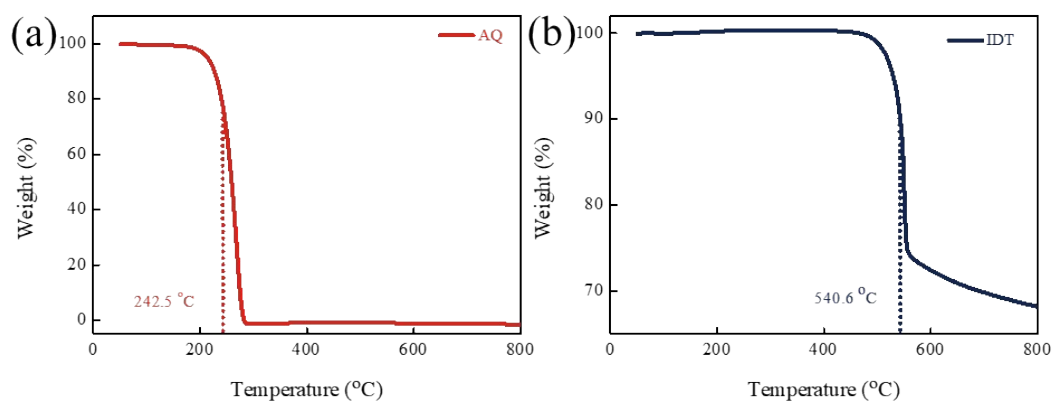
Fig. S5. TGA curves of AQ and IDT.
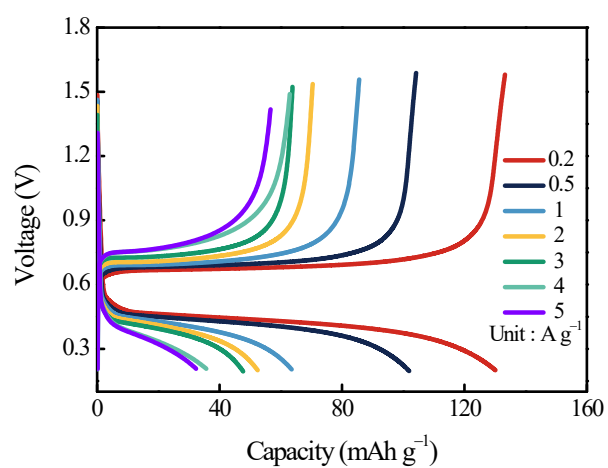
Fig. S6. GCD curves of AQ cathode.
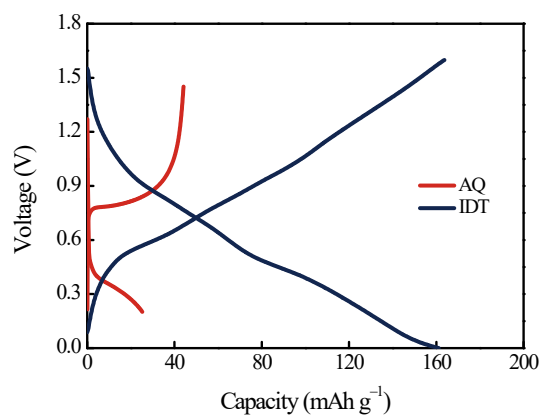
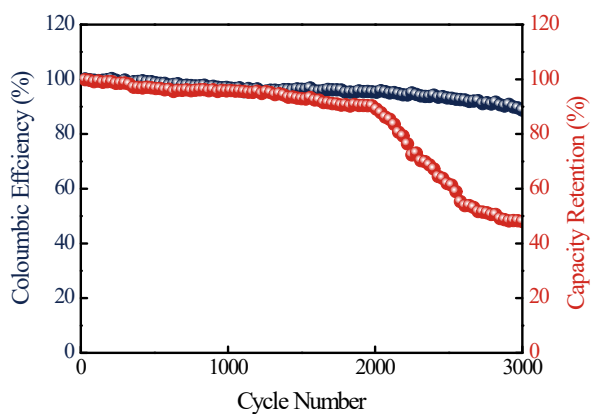**Fig. S7.** GCD curves of IDT and AQ cathodes at 10 A g^{-1}.

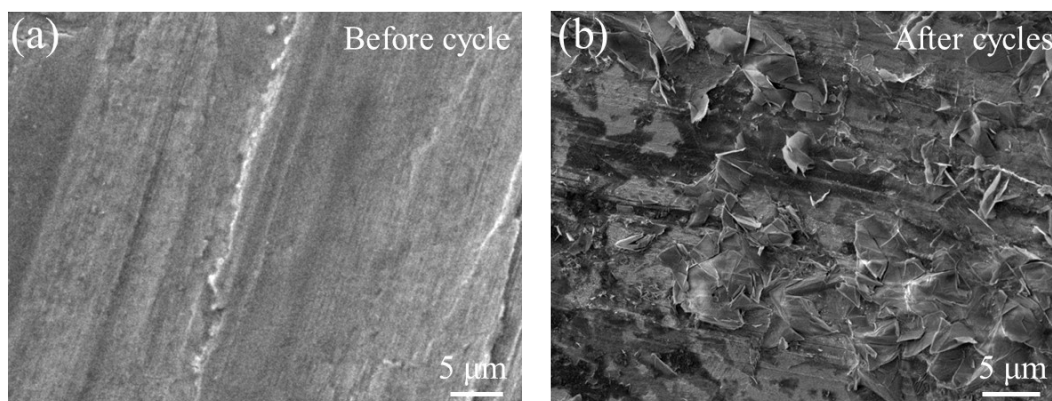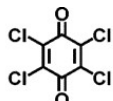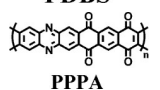**Fig. S8.** Cycling stability and corresponding coulombic efficiency of the Zn//AQ battery.
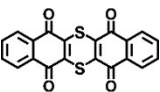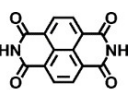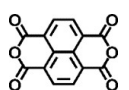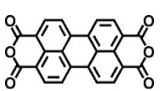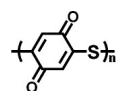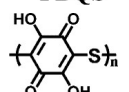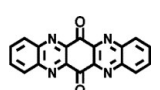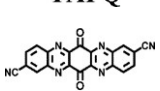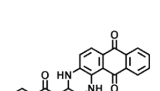

Fig. S9. SEM images of Zn anodes before and after cycles.

Table S1. Comparison of rate capacity, energy density and cycling performance of recently reported organic cathode materials for ZIBs in the literatures.

| Organic cathode	Electrolyte	Voltage (V)	Capacity (mAh g^{-1}/A g^{-1})	Retention (%) / (cycles)	Ref.
p-chloranil	1 M Zn(CF$_3$SO$_3$)$_2$	0.8-1.4	205 / 0.04	70 / 200 at 0.217 A g^{-1}	S10
DTT	2 M ZnSO$_4$	0.3-1.4	210.9 / 0.05	83.8 / 23 000 at 2 A g^{-1}	S11
NTCDI	2 M ZnSO$_4$	0.35-1.25	240 / 0.1	73.7 / 2000 at 1 A g^{-1}	S12
NTCDA	2 M ZnSO$_4$	0.35-1.25	170 / 0.1	-	S12
π-PMC	2 M ZnCl$_2$	0-1.0	122.9 / 0.2	68.2 / 1000 at 8 A g^{-1}	S13
PBQS	3 M Zn(CF$_3$SO$_3$)$_2$	0.2-1.8	203 / 0.02	86 / 50 at 0.04 A g^{-1}	S14
PDBS	2 M ZnSO$_4$	0.4-1.45	260 / 0.1	79 / 2000 at 2 A g^{-1}	S15
PPPA	2 M Zn(CF$_3$SO$_3$)$_2$	0.2-1.8	210.2 / 0.05	70.6 / 20, 000 at 5 A g^{-1}	S16
TAPQ	1 M ZnSO$_4$	0.1-1.6	443 / 0.05	50.2 / 100 at 0.05 A g^{-1}	S17
DCTPQ	2 M ZnSO$_4$	0.1-1.4	244 / 0.3	50 / 210 at 0.5 A g^{-1}	S18
IDT	**2 M Zn(CF$_3$SO$_3$)$_2$**	**0-1.6**	**238 / 0.2**	**88.7 / 3000 at 10 A g^{-1}**	**This work**
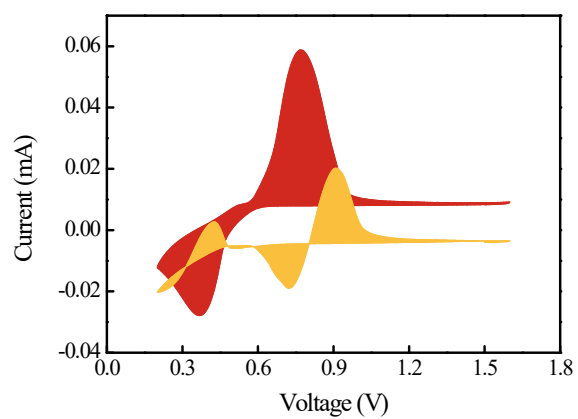
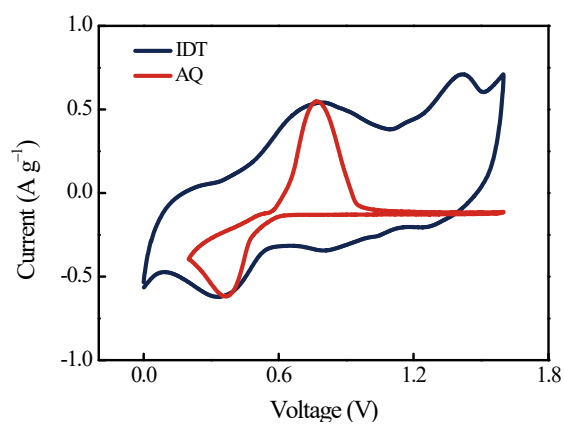**Fig. S10.** Capacitive contribution of the AQ cathode at 20 mV s^{-1}.
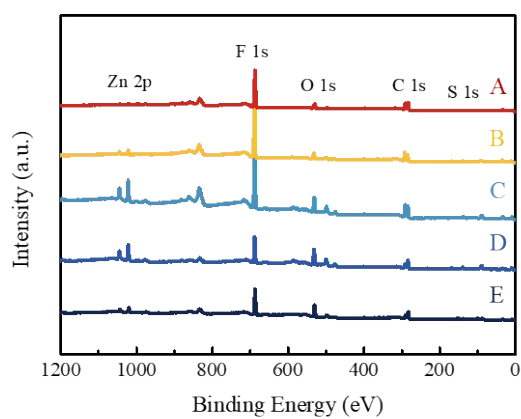

Fig. S11. CV curves of IDT and AQ.

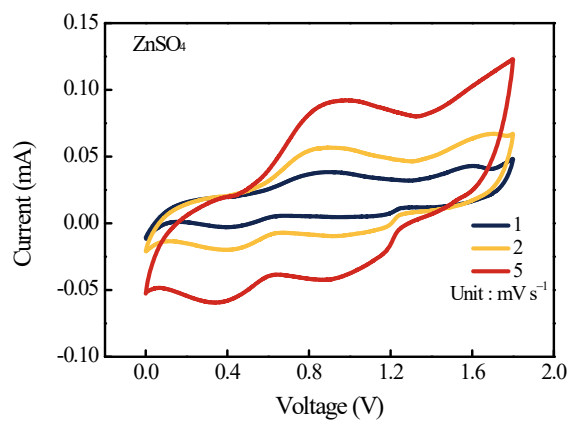**Fig. S12.** *Ex-situ* XPS spectra of IDT cathodes at various discharged/charged states.

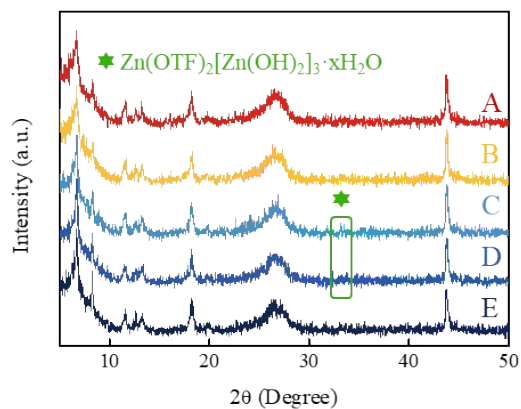**Fig. S13.** CV curves of IDT at ZnSO$_4$/H$_2$O electrolyte.
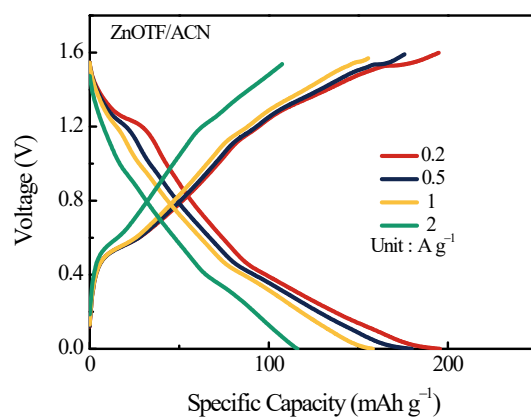

Fig. S14. *Ex-situ* XRD patterns.

Fig. S15. GCD curves of IDT cathode at 0.33 M Zn(OTF)$_2$/acetonitrile electrolyte.
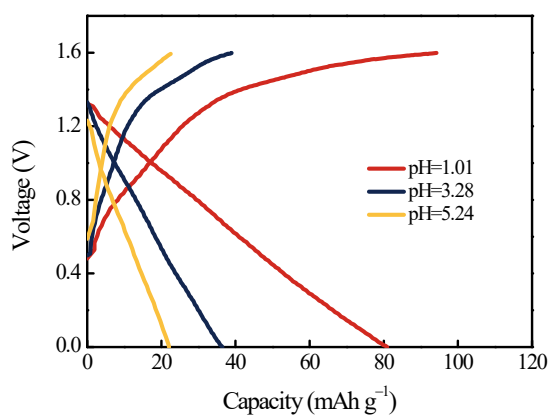
Fig. S16. GCD curves of IDT cathode at HOTF electrolytes with different pH values.
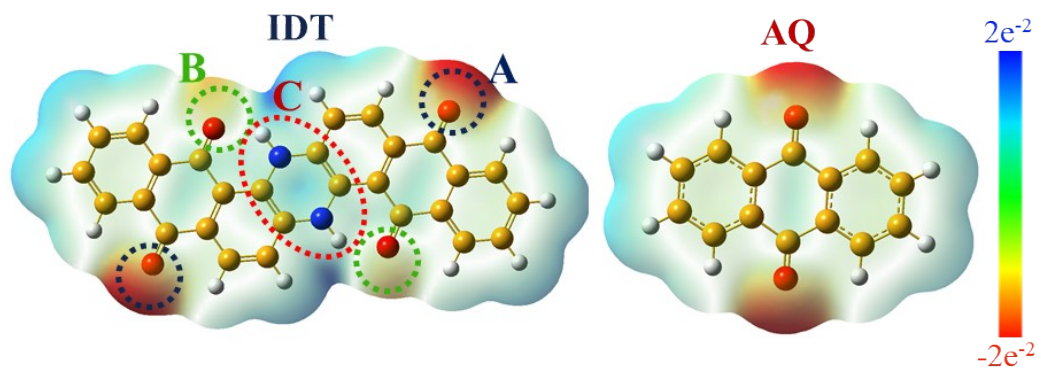

Fig. S17. ESP plots of IDT and AQ.

References

(S1) M. E. Casida, C. J., K. C. Casida. Molecular Excitation Energies to High-Lying Bound States from Time-Dependent Density-Functional Response Theory: Characterization, Correction of the Time-Dependent Local Density Approximation Ionization Threshold. *J. Chem. Phys.* **1996**, *108*, 4439-4449.

(S2) R. Bauernschmitt, R. A. Treatment of Electronic Excitations within the Adiabatic Approximation of Time Dependent Density Functional Theory. *Chem. Phys. Lett.* **1996**, *256*(4-5), 454-464.

(S3) M. J. Frisch, G. W. T., H. B. Schlegel, G. E. Scuseria, M. Robb, J. R. Cheeseman, H. Nakatsuji. Gaussian 09, Revision D. 01, Gaussian, Inc.:. *Wallingford, CT.* **2010**.

(S4) Becke, A. D. A New Mixing of Hartree-Fock, Local Density-Functional Theories. *J. Chem. Phys.* **1993**, *98*, 1372-1377.

(S5) Becke, A. D. Density-Functional Thermochemistry. Iii. The Role of Exact Exchange. *J. Chem. Phys.* **1993**, *98*(7), 5648-5652.

(S6) W. J. Hehre, R. D., J. A. Pople. Self-Consistent Molecular Orbital Methods. Xii. Further Extensions of Gaussian-

Type Basis Sets for Use in Molecular Orbital Studies of Organic Molecules. *J. Chem. Phys.* **1972**, *56*(5), 2257-2261.

(S7) P. C. Hariharan, J. A. P. The Influence of Polarization Functions on Molecular Orbital Hydrogenation Energies. *Theor. Chim. Acta* **1973**, *28*(3), 213-222.

(S8) M. M. Francl, W. J. P., W. J. Hehre, J. S. Binkley, M. S. Gordon, D. J. DeFrees, J. A. Pople. Self-Consistent Molecular Orbital Methods. Xxiii. A Polarization-Type Basis Set for Second-Row Elements. *J. Chem. Phys.* **1982**, *77*(7), 3654-3665.

(S9) T. Lu, F. C. Multiwfn: A Multifunctional Wavefunction Analyzer. *J. Comput. Chem.* **2012**, *33*, 580-592.

(S10) Kundu, D.; Oberholzer, P.; Glaros, C.; Bouzid, A.; Tervoort, E.; Pasquarello, A.; Niederberger, M. Organic Cathode for Aqueous Zn-Ion Batteries: Taming a Unique Phase Evolution toward Stable Electrochemical Cycling. *Chem. Mater.* **2018**, *30*(11), 3874-3881.

(S11) Wang, Y.; Wang, C.; Ni, Z.; Gu, Y.; Wang, B.; Guo, Z.; Wang, Z.; Bin, D.; Ma, J.; Wang, Y. Binding Zinc Ions by Carboxyl Groups from Adjacent Molecules toward Long-Life Aqueous Zinc-Organic Batteries. *Adv. Mater.* **2020**, *32*(16), e2000338.

(S12) Wang, X.; Chen, L.; Lu, F.; Liu, J.; Chen, X.; Shao, G. Boosting Aqueous Zn^{2+} Storage in 1,4,5,8-Naphthalenetetracarboxylic Dianhydride through Nitrogen Substitution. *ChemElectroChem* **2019**, *6*(14), 3644-3647.

(S13) Zhang, H.; Fang, Y.; Yang, F.; Liu, X.; Lu, X. Aromatic Organic Molecular Crystal with Enhanced π–π Stacking Interaction for Ultrafast Zn-Ion Storage. *Energy Environ. Sci.* **2020**, *13*(8), 2515-2523.

(S14) Dawut, G.; Lu, Y.; Miao, L.; Chen, J. High-Performance Rechargeable Aqueous Zn-Ion Batteries with a Poly(Benzoquinonyl Sulfide) Cathode. *Inorganic Chemistry Frontiers* **2018**, *5*(6), 1391-1396.

(S15) Sun, T.; Li, Z. J.; Zhi, Y. F.; Huang, Y. J.; Fan, H. J.; Zhang, Q. Poly(2,5-Dihydroxy-1,4-Benzoquinonyl Sulfide) as an Efficient Cathode for High-Performance Aqueous Zinc–Organic Batteries. *Adv. Funct. Mater.* **2021**, *31*(16).

(S16) Ye, F.; Liu, Q.; Dong, H.; Guan, K.; Chen, Z.; Ju, N.; Hu, L. Organic Zinc-Ion Battery: Planar, π-Conjugated Quinone-Based Polymer Endows Ultrafast Ion Diffusion Kinetics. *Angew. Chem. Int. Ed.* **2022**, *61*(51).

(S17) Gao, Y.; Li, G.; Wang, F.; Chu, J.; Yu, P.; Wang, B.; Zhan, H.; Song, Z. A High-Performance Aqueous Rechargeable Zinc Battery Based on Organic Cathode Integrating Quinone and Pyrazine. *Energy Storage Mater.* **2021**, *40*, 31-40.

(S18) Wang, Y.; Wang, X.; Tang, J.; Tang, W. A Quinoxalinophenazinedione Covalent Triazine Framework for Boosted High-Performance Aqueous Zinc-Ion Batteries. *J. Mater. Chem. A* **2022**, *10*(26), 13868-13875.